# An Approach for Predicting the Calibration Accuracy in Planar Cable-Driven Parallel Robots

Bozhao Wang, Philippe Cardou, Stéphane Caro

# An Approach for Predicting the Calibration Accuracy in Planar Cable-Driven Parallel Robots

Bozhao Wang, Philippe Cardou and Stéphane Caro

**Abstract** This paper presents a simulation of the calibration of a 3-DoF, 2-cable, planar cable-driven parallel robot (CDPR). The calibration is realized with the combination of a laser displacement sensor and an inclinometer attached to the moving platform. The actual accuracies of the sensors are tested at first for higher calibration quality. Through simulation, with more measurement poses used, the system variable identification errors are reduced, and have decreasing dispersion, finally form plateaus. The effect of each sensor on the calibration quality is studied. Based on the sensors considered in this work, the system variable errors are all within ±9 mm, and most are within ±5 mm for 5.209 m-span CDPR.

## 1 Introduction

Cable-driven parallel robots (CDPRs) are a group of parallel robots that are actuated through flexible cables instead of rigid links. Compared with serial robots, this particular type of robot benefits from its high flexibility, reconfigurability, and potentially large translational workspace. In most CDPRs, the moving platform (MP) is usually connected by several cables, then through pulleys, winches and then linked to the base frame. There are two configurations according to the number and spatial position of cables used: suspended and fully-constrained CDPRs [2].

Parallel mechanisms, because of their large numbers of links and passive joints [6], may not necessarily have a high accuracy. Therefore, kinematic calibration is important for such robot architectures. Daney et al. [8] used a method based on interval

Bozhao Wang and Stéphane Caro
CNRS, Laboratoire des Sciences du Numerique de Nantes, UMR CNRS 6004, 1, rue de la Noë, 44321 Nantes, France, e-mail: Bozhao.Wang@ls2n.fr, stephane.caro@ls2n.fr

Philippe Cardou
Laboratoire de robotique, Departement de génie mécanique, Université Laval, Québec, QC G1V 0A6, Canada, e-mail: Philippe.Cardou@gmc.ulaval.ca

arithmetics for kinematic parallel robot calibration. In [11], a high precision and robustness iterative calibration method is proposed to significantly improve the end-effector position errors. For CDPRs, most of previous works relied on non-linear least square (NLLS) methods for parameter identification, as it applies conveniently to the minimization of the cable length residuals. In [3], the NLLS method is used on a 6-cable, 3-degrees of freedom (DoF) CDPR, with a parallelogram, which is able to reach a larger workspace. The application is proven effective by simulations and experiments. The authors also proposed an algorithm to select optimal measurement poses. The authors of [1] used NLLS method for a CDPR called TBot and also considered pulley kinematics. They proposed a measurement pose optimization method, which consists in minimizing the identification matrix condition number. In [4], several identification methods derived from NLLS are proposed and tested. The other similiar approach is orthogonal distance regression (ODR) [14].

Sensors used for robot calibration can be divided into two catagories: exteroceptive and proprioceptive, which can be combined or not. Proprioceptive motor position sensors are used in [12] for auto-calibration. Zhang et al. [11] used only external measurement device to perform the iterative calibration method. Martin et al. [13] used laser-based cable length measurement sensor to improve calibration quality. Little research has been done on the combination of different types of sensors in CDPRs. Calibration with exteroceptive sensors has drawbacks such as low ratios between measurement accuracy and measurement volume, and the difficulty to access the end-effector in certain cases [5]. The use of proprioceptive sensors on the MP can mitigate those disadvantages. Renaud et al. [5] proposed to perform the kinematic calibration of a parallel mechanism by observing its legs with a camera, which can make the legs be observed more easily. The method combines the advantages of both exteroceptive and proprioceptive sensors. Andreff et al. [7] proposed kinematic calibration of a H4 parallel robot with computer vision. In ref. [8], Daney et al. used internal sensors to provide the leg length differences of a parallel mechanism.

This paper focuses on the simulation of the kinematic calibration for a 3-DoF, 2-cable, planar CDPR, using the combination of a laser displacement sensor and an inclinometer. Pulley kinematics is considered in the modelling. The intrinsic measurement errors of both sensors are examined beforehand to improve the calibration quality. Then the system variable identification errors are simulated based on the sensor measurement error after curve fitting. Besides, the effect of each sensor on the calibration quality is studied. The NLLS method is applied to minimize the cable length residual in order to identify the system parameters.

Section 2 focuses on the CDPR kinematic modelling and on accuracy. Section 3 describes the identification methodology of the current study. The obtained simulation results are discussed in Sec. 4, and then the conclusions are given.

## 2 CDPR Modelling

Figure 1(a) shows the CDPR base frame $\mathcal{F}_1$ and the real 3-DoF moving platform. Two pulleys in the diagonal direction are used, forming the CDPR workspace plane. The workspace frame is defined as $\mathcal{F}_2$, with a 5.2 m by 2.8 m size. $\mathcal{F}_2$ is built based on exit points in $\mathcal{F}_1$ that are measured accurately with a laser tracker. Cables are supposed to be inelastic, straight and massless. The robot geometry inside $\mathcal{F}_2$ can be seen in Fig. 1(b). The MP is a 0.5m-long straight bar. It is suspended by the two cables, which go through the two pulleys located near the cable exit points $A_1$ and $A_2$. The cables are then led to the motor winches fixed on the corresponding bottom corners in the base frame. The horizontal movement of the winch exit point because of cable coiling is neglected.

The MP will be equipped with an inclinometer and a laser displacement sensor connected to the the MP bar through a revolute joint. Thanks to this revolute joint, the laser sensor always points vertically to the ground, to directly measure the MP height. The total MP mass is 2.2 Kg. The ground is assumed to be flat, and is able to reflect enough laser light to perform proper measurements. Motors control the cable lengths, and are equipped with encoders that measure the motor angular position, and thus the cable-length variations.

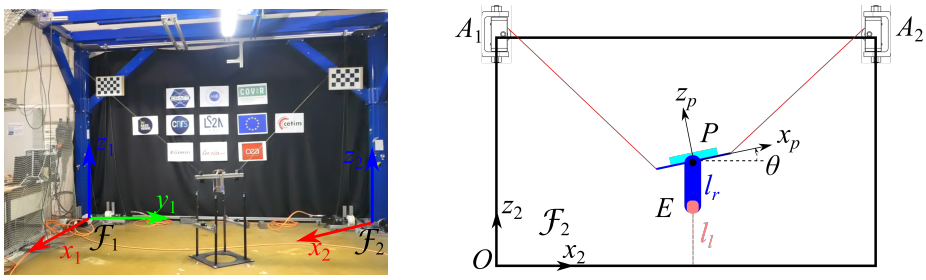


(a) MP in $\mathcal{F}_1$ and $\mathcal{F}_2$

(b) CDPR geometry inside $\mathcal{F}_2$

Fig. 1: CDPR under study equipped with a laser displacement sensor and an inclinometer

The MP has three DoF: one rotational and two translational DoF. However it is held by only two cables, which makes the robot under-constrained. With a certain set of cable lengths, the MP will always have one degree of freedom to move, but will eventually stay at the unique position where its gravitational potential energy is the smallest. The 50 poses used in the simulation and generated randomly are illustrated in Fig. 2.

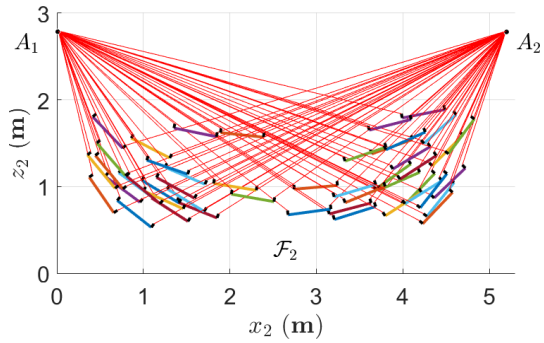


Fig. 2: Measurement poses randomly generated

## 2.1 Kinematic modelling

Figure 4 shows the $i$th loop of the current CDPR. The vectors pointing from the workspace origin $O$ to the $i$th pulley exit point and from $O$ to the MP center are $\mathbf{a}_i$ and $\mathbf{p}_j$, respectively; with $i = 1, \ldots, m$ and $j = 1, \ldots, n$ are the numbers of each cable and measurement poses, respectively. $m = 2$ and $n$ is the total number of measurement poses. Detailed pulley kinematic modelling is described in [2, 9] and is illustrated in Fig. 3. The vector from the pulley exit point $A'_i$ to the cable anchor point $B_i$ is $\mathbf{l}_{ci}$. The $j$th MP rotational angle compared with the horizontal plane is $\theta_j$. As a result, the cable length from the cable exit point $A_i$ to cable anchor point $B_i$ is:

$$l_{ti} = l_{pi} + l_{ci} \tag{1}$$

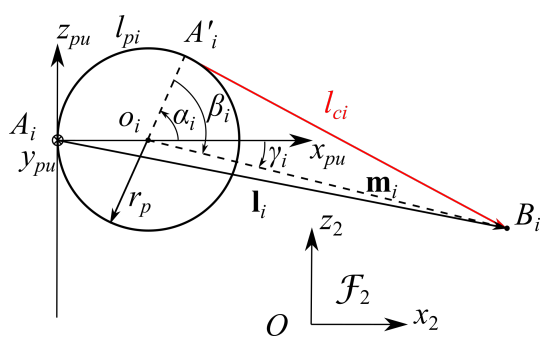


Fig. 3: Parameterization of the $i$th pulley

Following the $i$th loop of the CDPR geometry, $l_{ti}$ can be expressed as:

$$l_{ti} = r_p\left[\pi - \beta_i - \gamma_i\right] + \sqrt{\mathbf{m}_i\mathbf{m}_i^T - r_p^2} \tag{2}$$

where $r_p$ is the pulley radius, $\tan(\beta_i) = \frac{\sqrt{\mathbf{m}_i\mathbf{m}_i^T - r_p^2}}{r_p}$, $\sin(\gamma_i) = \frac{a_{iz} - b_{iz}}{||\mathbf{m}_i||_2}$, $\mathbf{m}_i = \mathbf{p} + \mathbf{b}_i - \mathbf{a}_i + r_p\,{}^b\mathbf{R}_i\mathbf{x}_{pu}$ is the vector pointing from the pulley center to the anchor point, $\mathbf{x}_{pu}$ is the unit vector along the $x$-axis of the pulley frame, and ${}^b\mathbf{R}_i$ is the rotation matrix from base frame to the pulley frame.

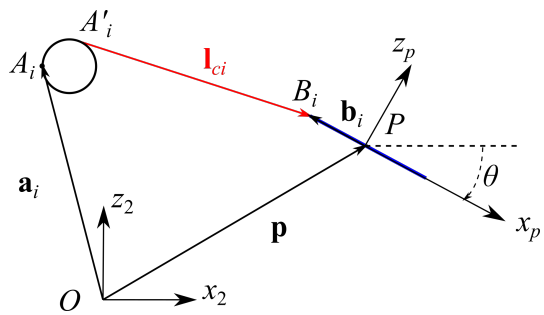


Fig. 4: The $i$th loop of the CDPR under study

## 2.2 Sensors accuracy test

Two sensors are considered in the simulation: the WitMotion BWT61CL inclinometer and the SICK DT50-2 laser displacement sensor. The calibration method in this work relies on the sensor measurements. Better knowledge on the measurements will certainly contribute to an improved calibration accuracy. Sensor measurements from both sensors are recorded and compared to the standard predefined angles and distances, respectively:

$$e_\theta = \theta_s - \theta_r, \quad e_d = d_s - d_r \tag{3}$$

where $e_\theta$ and $e_d$ are the actual measurement errors of the inclinometer and the laser displacement sensor, $\theta_s$ and $d_s$ are the sensor output measurements from both sensors, $\theta_r$ and $d_r$ are the standard predefined measurement values for both sensors.

Measurement curve fitting for both sensors are conducted. The $\sec(\theta_j)$ with a constant ratio between lateral and gravitational acceleration $\frac{da}{g} = -0.24$ fits $e_\theta$ the best. As $e_d$ is roughly uniformly distributed, its mean value $e_{d,fit}$ is used over its full range. Regarding the realistic poses, the ranges lower than 60° for the inclinometer and less than 3000 mm for the displacement sensor are considered. From the test, the inclinometer accuracy is determined as ± 0.1° with 0.05° repeatability, and the laser displacement sensor accuracy is ± 6 mm with a 1.5 mm repeatability.

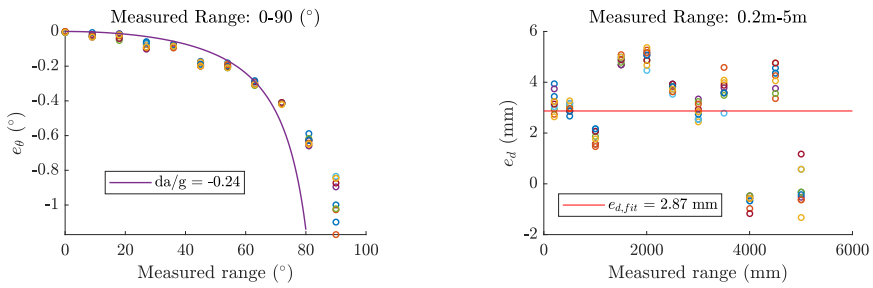


(a) Inclinometer accuracy

(b) Laser displacement sensor accuracy

Fig. 5: WitMotion BWT61CL inclinometer and SICK DT50-2 laser displacement sensor accuracy measurements

## 3 Identification methodology

The robot calibration is achieved with the information from all the sensors throughout all the MP measurement poses. At the initial position, the cable lengths are denoted as $l_{i0}$. When the MP is moved to all the $n$ different poses within the workspace, the cable length variations $\Delta l_{ij}$ are recorded by the encoders. Thus, the actual cable lengths $l_{ij}$ are calculated by:

$$l_{ij} = \Delta l_{ij} + l_{i0} \tag{4}$$

The CDPR system variables are the outputs of the problem, including the Cartesian coordinates of cable exit points $a_{ix}, a_{iz}$, the initial cable lengths $l_{i0}$, the Cartesian coordinates of the MP center $p_{jx}$, $p_{jz}$ and the MP rotation angle $\theta_j$. Among these variables, the laser displacement sensor measures $p_{jz}$, and the inclinometer measures $\theta_j$. All the sensor measurements are the inputs of the identification problem. The rest of the output variables are considered to be the problem unknowns, included in a $3m + n$ dimensional vector $\mathbf{x}$:

$$\mathbf{x} = [a_{1x}\, a_{1z}\, a_{2x}\, a_{2z}\, l_{10}\, l_{20}\, p_{1x} \ldots p_{nx}]^T \tag{5}$$

Between the real cable length $l_{ij}$ from Eq.(4) and the estimated cable lengths $l_{ti}$ from Eq.(2), a system of $mn$ equations can be obtained [2, 10]:

$$f_{ij}(\mathbf{x}) = (l_{pi} + l_{ci})^2 - (\Delta l_{ij} + l_{i0})^2, \quad i = 1, 2 \quad , j = 1, \ldots, n \tag{6}$$

To solve the nonlinear system of equations defined by Eq.(6), the number of inputs must be larger than or equal to the number of unknowns:

$$mn + 2n \geq 2m + m + 3n \tag{7}$$

As the CDPR has $m = 2$ cables, the least number of measurement poses is $n = 6$. A similar simulation process is used in [9, 10]. Arbitrary errors are added on $\mathbf{x}$ to simulate the approximately known system variables. The identification problem is then formulated as the non-linear least square problem in Eq.(8):

$$\min_{\mathbf{x}} \left( \sum_{i=1}^{m} \sum_{j=1}^{n} f_{ij}^2 \right) \tag{8}$$

The pre-defined real variable values $\mathbf{x}_r$ are compared with the identified ones $\mathbf{x}^*$, to evaluate the identification quality:

$$\delta \mathbf{x}_k = \mathbf{x}_k^* - \mathbf{x}_{r,k}, \qquad k = 1, 2, ..., 3m + n \tag{9}$$

where $\delta \mathbf{x}_k$ is the difference between the real and identified variable values.

## 4 Simulation of 3-DoF, 2-cable planar CDPR

### 4.1 Results of the simulated identification problem

Simulations with 6 to 50 measurement poses are performed. For each pose, the simulation is repeated 500 times with different sensor measurement errors. Based on the accuracy test results given in Sec.2, the applied accuracy and repeatability are generated as normally distributed values, assuming the sensor accuracy and repeatability ranges as three times the standard deviation, and zero distribution mean.

The dispersion or standard deviations of the obtained results $\delta \mathbf{x}_k$ is defined as:

$$\sigma = std(\delta \mathbf{x}_k), \qquad k = 1, 2, ..., 3m + n \tag{10}$$

Figure 6 shows $\sigma$ of the $x$-coordinate of the 2nd cable exit point, the initial cable length of the 1st cable and the x-coordinate of the 4th MP pose. It is apparent that the higher the number of poses, the lower the $\sigma$, the better the geometric calibration quality. It should be noted that $\sigma$ does not decrease after 50 measurement poses.

Figures 7 to 9 are the summary of three examples of the identification errors of the system variables with different number of measurement poses used, and the $\sigma$ of the identified values are shown. The results are plotted as probability density function (PDF). It can be seen that the higher the number of poses (from 6 to 50), the lower the system variable identification errors. When only six poses are used, the probability density function plots are quite flat, the errors are bounded between -50 and 50 mm. Afterwards, the PDF plots tend towards normal distributions, the main part of the identification errors is distributed in the lower value area. Besides, the $\sigma$ values keep decreasing as the number of measurement poses increases, which means that the identification error dispersion becomes lower and the identification quality is higher.

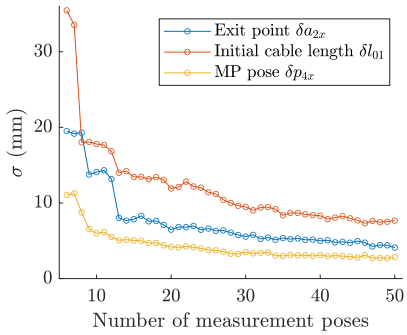


Fig. 6: The $\sigma$ results of 3 examples of the system variables

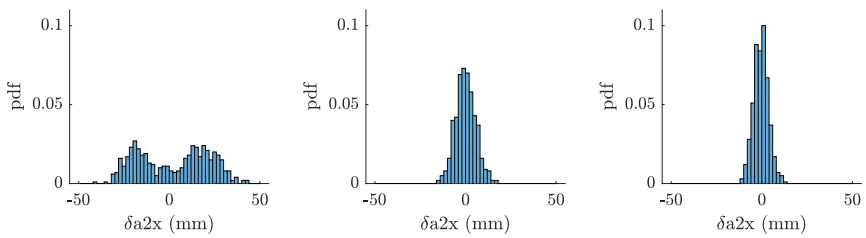


(a) 6 poses, $\sigma$=19.5003 mm (b) 30 poses, $\sigma$=5.5474 mm (c) 50 poses, $\sigma$=4.0962 mm

Fig. 7: Identification error results in the $x$-coordinates of the 2nd cable exit point, with different number of measurement poses and $\sigma$ values

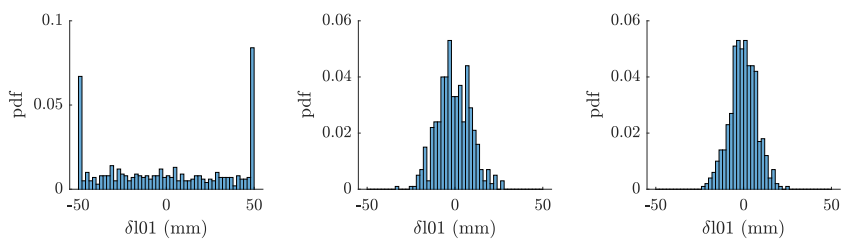


(a) 6 poses, $\sigma$=35.4669 mm (b) 30 poses, $\sigma$=9.4841 mm (c) 50 poses, $\sigma$=7.6688 mm

Fig. 8: Identification error results of the initial length in the 1st cable, with different number of measurement poses and $\sigma$ values

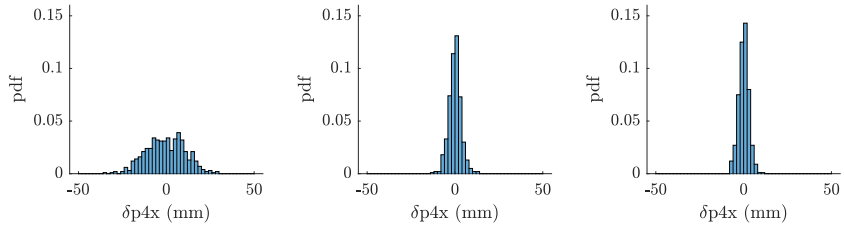


(a) 6 poses, $\sigma$=11.0545 mm (b) 30 poses, $\sigma$=3.4903 mm (c) 50 poses, $\sigma$=2.8290 mm

Fig. 9: Identification error results of the $x$-coordinates of the 4th MP position vector, with different number of measurement poses and $\sigma$ values

In general, from the identification error results, the variables of MP coordinates have the lowest errors, with nearly all the values below 10 mm and the minimum $\sigma$ being 2.8290 mm. The errors in the coordinates of exit point come next, the maximum identification errors slightly exceeding 15 mm, and the minimum $\sigma$ value being 4.0962 mm. The initial cable lengths have the largest errors, with the maximum values around 25 mm and minimum $\sigma$ value being 7.6688 mm.

## 4.2 Simulation of sensor effects on identification errors

The two sensors provide different types of quantities (lengths and angles), which makes the effect of each sensor on the overall calibration quality difficult to discern. Therefore, the simulations when eliminating each of the sensor measurement errors one at a time are carried out. If one sensor is eliminated, its measurement error will be set to zero, and the simulation will be processed by considering the errors in the other sensor only.

An example of this set of results for the 2nd exit point $x$-coordinate $a_{2x}$ is shown in Fig. 10. As a result, when the SICK sensor measurement errors are eliminated, the identification errors are much reduced, the dispersion of the 500 results are significantly reduced, as shown in Fig. 10(c). The identification errors are much more concentrated around 0 mm, and within ± 6 mm. And the $\sigma$ values decreased from 7.4969 mm to 0.2145 mm. In comparison, the errors for the $x$-coordinates of initial cable lengths are even more affected, with identification errors inside ± 1 mm range. It should be noted that the errors in the $x$-coordinates of the MP positions are less affected, reduced from ±10 mm to ±5 mm.

On the other hand, when the WitMotion inclinometer is not considered, the identification errors do not really change as shown in Fig. 10(b). The elimination of inclinometer measurement errors does not improve much the identification quality. It means that the identification quality of the geometric parameters of the planar

CDPR, the initial cable lengths and the moving-platform poses are not very sensitive to measurement errors in WitMotion inclinometer.

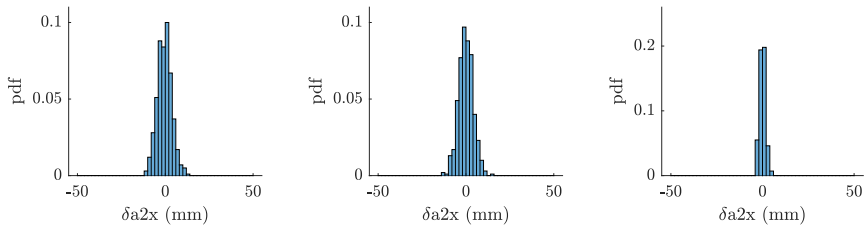


(a) Both sensors, $\sigma$=4.0962mm (b) SICK sensor, $\sigma$=4.1247mm (c) Inclinometer, $\sigma$=1.6193mm

Fig. 10: Identification error results in the $x$-coordinates of the 2nd exit point when 50 poses are used, comparison of sensor effects

## 4.3 Overall simulation

The previous sections explained in detail different factors that affect overall identification quality. In this section, the overall simulation regarding the realistic experiment process is discussed. Similar to previous simulations, the same sensor measurement errors are applied. One single calibration using all the 50 measurement poses is performed. Identification errors $\delta\mathbf{x}$, i.e. the differences between the identified and real system variables are calculated. MP movement is also simulated, the control scheme code that will be able to move the real robot is used in the simulation. The overall simulation result is shown in Fig. 11. All identification errors fall within the range of ±9 mm, which is consistent with the previous detailed simulation. Besides, among the identification errors, 89.8% are less than ±5 mm.

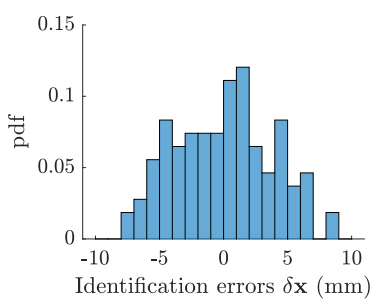


Fig. 11: Identification errors in all system variables

## 5 Conclusions and Future Work

This paper presented the simulation of the calibration of a 3-DoF, 2-cable, planar CDPR. In addition to motor encoders, the calibration relies on the combination of a laser displacement sensor and an inclinometer embedded on the moving platform. Detailed pulley kinematics are considered. The actual accuracies of the sensors are examined beforehand. The simulations showed that with more measurement poses used, the identification errors of the exit point, pose Cartesian coordinates and the initial cable lengths were reduced, and were less dispersed. It turns out that the laser displacement sensor has a much larger influence than the inclinometer on the identification errors. Furthermore, amongst all system variables, the errors in initial cable lengths are the most sensitive to the laser displacement sensor measurement errors whereas the errors in the MP position coordinates are the least sensitive ones. Based on the sensor considered in this work, the system variable errors are all below ±9 mm, and most are below ±5 mm.

Later on, experimental validations will be carried out. In addition to pulley kinematics, cable elasticity and mass will be considered to improve calibration quality. Future work will also deal with the determination of optimal measurement poses for CDPR calibration.

**Acknowledgements** This work was supported by the ANR CRAFT project, grant ANR-18-CE10-0004, https://anr.fr/Project-ANR-18-CE10-0004. Bozhao Wang is grateful for the support of China Scholarship Council (CSC Grant No.202008070051).

## References

1. Zhang, Z., Xie, G., Shao, Z. & Gosselin, C. Kinematic Calibration of Cable-Driven Parallel Robots Considering the Pulley Kinematics. *Mechanism And Machine Theory*. **169** (2022)
2. Picard, E., Caro, S., Claveau, F. & Plestan, F. Pulleys and Force Sensors Influence on Payload Estimation of Cable-Driven Parallel Robots. *2018 IEEE/RSJ International Conference On Intelligent Robots And Systems (IROS 2018)*. (2018,10), https://hal.archives-ouvertes.fr/hal-01862015
3. Qian, S., Bao, K., Zi, B. & Wang, N. Kinematic calibration of a cable-driven parallel robot for 3D printing. *Sensors (Switzerland)*. **18** (2018)
4. Sandretto, J., Daney, D. & Gouttefarde, M. Calibration of a Fully-Constrained Parallel Cable-Driven Robot. *CISM International Centre For Mechanical Sciences, Courses And Lectures*. **544**, 77-84 (2013)
5. Renaud, P., Andreff, N., Martinet, P. & Gogu, G. Kinematic calibration of parallel mechanisms: A novel approach using legs observation. *IEEE Transactions On Robotics*. **21**, 529-538 (2005)
6. Wang, J. & Masory, O. On the accuracy of a Stewart platform. I. The effect of manufacturing tolerances. *[1993] Proceedings IEEE International Conference On Robotics And Automation*. pp. 114-120 vol.1 (1993)
7. Andreff, N., Renaud, P., Martinet, P. & Pierrot, F. Vision-based kinematic calibration of an H4 parallel mechanism: Practical accuracies. *Industrial Robot*. **31**, 273-283 (2004)
8. Daney, D., Papegay, Y. & Neumaier, A. Interval methods for certification of the kinematic calibration of parallel robots. *Proceedings - IEEE International Conference On Robotics And Automation*. **2004**, 1913-1918 (2004)

9. Wang, B. & Caro, S. Exit Point, Initial Length and Pose Self-calibration Method for Cable-Driven Parallel Robots. *Mechanisms And Machine Science*. **103**, 90-101 (2021)
10. Fortin-Côté, A., Cardou, P. & Gosselin, C. An admittance control scheme for haptic interfaces based on cable-driven parallel mechanisms. *Proceedings - IEEE International Conference On Robotics And Automation*. pp. 819-825 (2014)
11. Zhang, F., Shang, W., Li, G. & Cong, S. Calibration of geometric parameters and error compensation of non-geometric parameters for cable-driven parallel robots. *Mechatronics*. **77**, 102595 (2021), https://doi.org/10.1016/j.mechatronics.2021.102595
12. Miermeister, P., Pott, A. & Verl, A. Auto-calibration method for overconstrained cable-driven parallel robots. *7th German Conference On Robotics, ROBOTIK 2012*., 301-306 (2012)
13. Martin, C., Fabritius, M., Stoll, J. & Pott, A. A laser-based direct cable length measurement sensor for CDPRS. *Robotics*. **10**, 1-11 (2021)
14. Boggs, P., Byrd, R. & Schnabel, R. A Stable and Efficient Algorithm for Nonlinear Orthogonal Distance Regression. *SIAM J. Sci. Stat. Comput.*. **8**, 1052-1078 (1987,11), https://doi.org/10.1137/0908085